PCCP

ROYAL SOCIETY OF CHEMISTRY

PAPER

View Article Online
View Journal | View Issue

Cite this: *Phys. Chem. Chem. Phys.*, 2024, **26**, 5640

Electron-triggered processes in halogenated carboxylates: dissociation pathways in CF_3COCl and its clusters†

Barbora Kocábková, ‡[a] Jozef Ďurana, ‡[a] Jozef Rakovský, [a] Andrij Pysanenko, [a] Juraj Fedor, [a] Milan Ončák *[b] and Michal Fárník *[a]

Received 6th November 2023,
Accepted 15th January 2024

DOI: 10.1039/d3cp05387c

rsc.li/pccp

Trifluoroacetyl chloride, CF_3COCl, is produced in the Earth's atmosphere by photooxidative degradation of hydrochlorofluorocarbons, and represents a potential source of highly reactive halogen radicals. Despite considerable insight into photochemistry of CF_3COCl, its reactivity towards electrons has not been addressed so far. We investigate the electron ionization and attachment in isolated CF_3COCl molecules and $(CF_3COCl)_N$, max. $N \geq 10$, clusters using a molecular beam experiment in combination with quantum chemical calculations. The ionization of the molecule at 70 eV electron energy leads to strong fragmentation: weakening of the C–C bond yields the CF_3^+ and $COCl^+$ ions, while the fission of the C–Cl bond produces the major CF_3CO^+ fragment ion. The cluster spectra are dominated by $M_n{\cdot}COCl^+$ and $M_n{\cdot}CF_3CO^+$ ions (M = CF_3COCl). The electron attachment at energies between 1.5 and 11 eV also leads to the dissociation of the molecule breaking either the C–Cl bond at low energies below 3 eV yielding mainly Cl^- ions, or dissociating the C–C bond at higher energies above 4 eV leading mainly to CF_3^- ions. In the clusters, the intact M_n^- ions are stabilized after electron attachment at low energies with contribution of $M_n{\cdot}Cl^-$ fragment ions. At higher energies, the $M_n{\cdot}Cl^-$ fragments dominate the spectra, and C–C bond dissociation occurs as well yielding $M_n{\cdot}CF_3^-$. Interestingly, $M_n{\cdot}Cl_2^-$ ions appear in the spectra at higher energies. We briefly discuss possible atmospheric implications.

1 Introduction

Certain ozone-depleting chlorofluorocarbons (CFCs) nowadays have been largely replaced by hydrochlorofluorocarbons (HCFCs). Chemicals within this class of compounds are considered to be acceptable temporary alternatives to CFCs[1,2] (according to the Montreal Protocol, the definite phase-out of HCFCs is foreseen in 2030). HCFCs undergo further reactions in the atmosphere. Their photooxidative degradation produces trifluoroacetyl chloride (TFAC, CF_3COCl).[3,4] Since CF_3COCl is a potential source of highly reactive halogen radicals, its presence in the atmosphere creates a need for understanding the dissociation pathways of this molecule.

A lot of attention has been dedicated recently to the dissociation of CF_3COCl induced by UV photons[3–11] and its photochemical pathways are thus well understood. Its structure as well as vibrational spectra were also analyzed both experimentally[12–14] and theoretically.[15] There is, however, no information about electron-induced dissociation of CF_3COCl – even the electron ionization mass spectrum is not available in the NIST database. At the same time, energetic particle precipitation influences chemical changes in the atmosphere.[16] Each type of naturally occurring ionizing radiation – galactic cosmic rays, solar energetic particles and energetic electron precipitation – produces an avalanche of secondary electrons[16] which can effectively induce molecular dissociation.[17] For example, cosmic-ray driven electron-induced reactions of CFCs have been proposed to contribute considerably to ozone depletion.[18,19] They have been even suggested to be a driving force behind climate change,[20,21] however, this hypothesis has met with strong criticism.[22,23] These proposed roles of halogenated species motivate the need for addressing our complete lack of knowledge about the electron-induced chemistry of HCFCs and the current target, TFAC. In this respect, CF_3COCl

[a] *J. Heyrovský Institute of Physical Chemistry, v.v.i., Czech Academy of Sciences, Dolejškova 2155/3, 18223 Prague 8, Czech Republic. E-mail: michal.farnik@jh-inst.cas.cz*
[b] *Institut für Ionenphysik und Angewandte Physik, Universität Innsbruck, Technikerstraße 25, 6020 Innsbruck, Austria. E-mail: milan.oncak@uibk.ac.at*

† Electronic supplementary information (ESI) available: Detailed mass spectra of positive and negative ions, isotopologue analysis for positive and negative ions, results of genetic algorithm optimizations, Cartesian coordinates of all optimized structures. See DOI: https://doi.org/10.1039/d3cp05387c

‡ Also affiliated to the University of Chemistry and Technology, Technická 5, Prague 6, 166 28, Czech Republic.

is interesting also from the chemical perspective due to the presence of five highly electronegative atoms, contributing to its considerable reactivity and possible instability upon ionization/electron attachment.

Similarly, there is no information available about how the aggregation of CF_3COCl influences its dissociation. This is relevant since heterogeneous processes, especially occurring on aerosol nanoparticles, are crucial for chemical transformations in the atmosphere. In laboratory investigations, such aerosols can be mimicked by clusters in molecular beams.[24] Apart from elucidating the atmospheric pathways, the cluster-beam studies offer the possibility of probing the gas-phase and aggregated molecules with exactly the same experimental techniques which facilitates the identification of dissociation mechanisms.[25]

In this study, we investigate the electron-induced dissociation of isolated CF_3COCl molecules and their clusters. We probed both the cationic pathways, induced by electrons with 70 eV kinetic energy, and anionic pathways, induced by the attachment of slow (less than 11 eV) electrons. We focus especially on the dissociative processes and how they are influenced by clustering. The experiments are complemented by quantum chemical calculations to provide insight into the structure, energetics and dissociation pathways of both single-molecular ions and clusters.

2 Methods

2.1 Experiment

The experiments were performed with the cluster-beam (CLUB) apparatus in Prague, the general description of which can be found in our recent reviews[24–26] and references cited therein. The beams of CF_3COCl molecules and clusters in a vacuum were generated by continuous supersonic expansions of CF_3COCl with helium and argon buffer gas, respectively. A 5% (by the partial pressure) mixture of CF_3COCl with the buffer gas was prepared in a pressurized cylinder and the gas mixture was expanded at a constant pressure p_S through a conical nozzle (50 μm diameter, 30° full opening angle, and 2 mm long). Different expansion pressures p_S were exploited for optimum cluster generation discussed below.

About 2.5 cm downstream from the nozzle, the beam passed through a skimmer (0.8 mm diameter) into the next differentially pumped vacuum chamber and subsequently passed through two additional chambers on a flight path of about 1.5 m before entering a reflectron time-of-flight mass spectrometer (TOF-MS) chamber for the cluster ionization and detection. Our TOF-MS was first described elsewhere.[27,28] It can detect either positive ions as described in the above cited publications, or it can work in the negative ion mode.[29,30] Here, we use both modes. The clusters are ionized by an electron beam pulsed at 10 kHz frequency. The positive ions were generated by 70 eV electrons. Since we have not found the mass spectrum of the CF_3COCl molecule in the NIST database, where the standard mass spectra measured at 70 eV electron energy can be found, we have measured the mass spectrum at this energy to provide the standard spectrum. The ionization pulse width was 5 μs. After a 0.5 μs delay, the ions were extracted by a 4 kV pulse and further accelerated to 8 keV into the time-of-flight region. In the negative ion mode, the electron energy was scanned from 0 to 11 eV in steps of 0.2 eV. The same settings were used with the voltages of opposite polarities. After the flight path of approximately 95 cm in the reflectron TOF-MS, the ions were detected with a microchannel plate detector and the mass spectra were recorded.

It ought to be mentioned that our electron source was not designed specifically for producing low-energy electrons, therefore our electron energy dependent ion yields provide reliable values at energies higher than approximately 1.5 eV.[29,30] The electron energy scale was calibrated using 4.4 eV and 8.2 eV resonances in dissociative electron attachment to CO_2 molecules.

From the combination of the positive and negative ion mass spectra generated from the same cluster beam, some information about the neutral cluster size distribution can be derived (see the ESI†). For the present experiment we estimate that the $(CF_3COCl)_N$ clusters in the beam have maximum sizes, only slightly larger than $N \geq 10$.

2.2 Theory

The structure of all molecules and ions was optimized at the B3LYP-D3/aug-cc-pVTZ level of theory employing the D3 dispersion correction as proposed by Grimme.[31] To obtain more reliable electronic energies, single-point recalculation at the coupled cluster singles and doubles level, also with non-iteratively included triplets, CCSD/aug-cc-pVDZ and CCSD(T)/aug-cc-pVDZ, respectively, was performed, with the zero-point energy included as calculated at the B3LYP-D3/aug-cc-pVTZ level (when not stated otherwise, we refer to CCSD(T) values in the text). We include both CCSD and CCSD(T) reaction energies as CCSD(T) calculations were too demanding in the case of trimer clusters. Charges on atoms were calculated employing the CHELPG scheme at the B3LYP-D3/aug-cc-pVTZ level.[32] Wave function stabilization was performed prior to every calculation. A search for the structure of neutral and charged CF_3COCl dimers, trimers and tetramers was performed using our in-house genetic algorithm code.[33] Namely, we create a pool of 20 initial structures and run 20 (dimers) and 30 (trimers, tetramers) cycles with 10 recombinations in each. The semi-empirical PM6 approach was used within genetic algorithm runs, 30 structures were subsequently re-optimized at BLYP-D3/6-31g* and B3LYP-D3/aug-cc-pVDZ levels to select four most stable or representative structures. For a cationic tetramer, two runs with 16 cycles were performed due to convergence issues. Tetramer structures were calculated only up to the B3LYP-D3/aug-cc-pVDZ level and are summarized in the ESI.† Although the employed technique is incapable of providing an exhaustive exploration of the rich potential energy surface of the investigated species, it offers an overview of its most important features as discussed below. All quantum chemical calculations were performed using the Gaussian 16 program.[34]

3 Results and discussion

3.1 Neutral cluster structure

We start our discussion with the calculated structures of the neutral CF_3COCl molecule and its molecular clusters, see Fig. 1a. The CF_3COCl molecule is calculated to have C_s symmetry, the highest negative charge is predicted on the oxygen atom, $-0.33e$, fluorine atoms have a charge of about $-0.2e$. The calculated structure shows eclipsed configuration of CF_3 with respect to the CO group, in agreement with the structure determined by electron diffraction.[14]

When complexed in a dimer, the most stable structure found is $OCF_2\cdots CF_3$ CFClCOCl, *i.e.*, with considerable rearrangement of the two CF_3COCl units. Such reorganization is a typical feature of the highly reactive CF_3COCl molecules as will be also discussed below. However, we do not expect this structure to be present in the experiment due to kinetic reasons. Considering a simple $(CF_3COCl)_2$ dimer structure, the most stable structure maximizes the interaction between CF_3 and COCl groups, probably due to slight polarization of the groups, with the COCl group becoming slightly negatively charged. For neutral trimers and tetramers, clusters with intact CF_3COCl units are predicted to be the most stable ones (see ESI,† for tetramers). However, the presence of, *e.g.*, the $(CF_3COCl)_2{\cdot}CF_3Cl{\cdot}CO$ structure among the most stable trimer isomers further emphasises the low thermodynamic stability of the CF_3COCl molecule with highly electronegative atoms.

3.2 Positive ions

Fig. 2 shows the positive ion mass spectrum of the CF_3COCl molecule in co-expansion with helium, measured at 70 eV electron energy. To our best knowledge, no mass spectrum of the gas phase molecule could be found in the literature. The molecule fragments significantly upon the ionization exhibiting only very little abundance of the parent ion CF_3COCl^+ at m/z = 132. The major fragment ions (in order of their abundances) are: CF_3CO^+ (m/z = 97), CF_3^+ (69), $COCl^+$ (63), CF_2Cl^+ (85) and CF_2^+ (50).

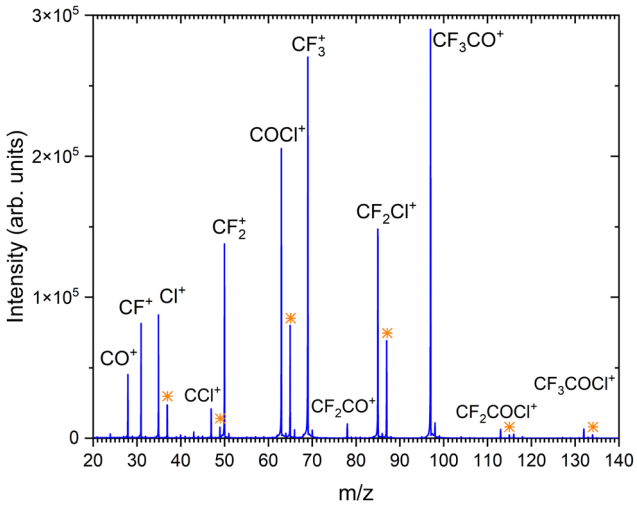

Fig. 2 The mass spectrum of CF_3COCl molecule at 70 eV electron energy. The assigned ions are indicated and the isotope peaks corresponding to the isotpe ^{37}Cl are labeled by the orange stars.

Our calculations show that the vertical and adiabatic ionization energies of the CF_3COCl molecule are 12.6 eV and 11.6 eV, respectively. In the cation ground state, the electron is removed from an orbital localized mostly on the C–C bond. Subsequently,

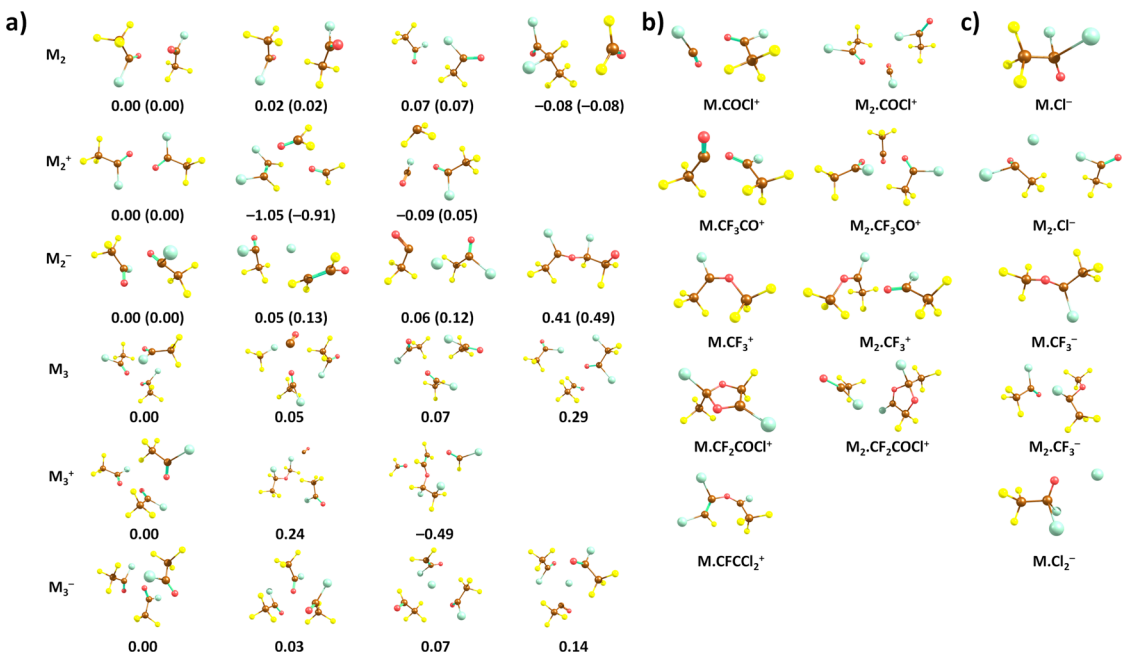

Fig. 1 Optimized (a) neutral and positively and negatively charged dimers and trimers of CF_3COCl and (b) cationic and (c) anionic fragments. For clusters, zero of energy is set to the structure considered to be present in the experiment, energy is given in eV. Calculated at the CCSD/aug-cc-pVDZ//B3LYP-D3/aug-cc-pVTZ level, the CCSD(T)/aug-cc-pVDZ//B3LYP-D3/aug-cc-pVTZ values are given in parentheses.

Table 1 Energies of various reactions including CF_3COCl. Calculated at the CCSD/aug-cc-pVDZ//B3LYP-D3/aug-cc-pVTZ level, CCSD(T)/aug-cc-pVDZ//B3LYP-D3/aug-cc-pVTZ values are given in parenthesis. For reactions with oligomers, clusters with zero relative energy in Fig. 1 are used

Reaction	Energy (eV)
$2CF_3COCl \rightarrow (CF_3COCl)_2$	−0.19 (−0.23)
$3CF_3COCl \rightarrow (CF_3COCl)_3$	−0.48
$CF_3COCl \rightarrow CF_3COCl^+ + e^-$	11.68 (11.62)
$(CF_3COCl)_2 \rightarrow (CF_3COCl)_2^+ + e^-$	11.29 (11.18)
$(CF_3COCl)_3 \rightarrow (CF_3COCl)_3^+ + e^-$	11.07
$CF_3COCl + e^- \rightarrow CF_3COCl^-$	−1.00 (−1.04)
$(CF_3COCl)_2 + e^- \rightarrow (CF_3COCl)_2^-$	−1.32 (−1.43)
$(CF_3COCl)_3 + e^- \rightarrow (CF_3COCl)_3^-$	−1.58
$CF_3COCl^+ \rightarrow CF_3CO^+ + Cl$	0.04 (0.20)
$CF_3COCl^+ \rightarrow CF_3^+ + COCl$	0.88 (0.96)
$CF_3COCl^+ \rightarrow COCl^+ + CF_3$	0.08 (0.18)
$CF_3COCl^+ \rightarrow CF_2Cl^+ + OCF$	0.74 (0.81)
$CF_3COCl^+ \rightarrow CF_2^+ + COClF$	2.01 (2.10)
$(CF_3COCl)_2^+ \rightarrow CF_3COCl{\cdot}COCl^+ + CF_3$	0.13 (0.29)
$(CF_3COCl)_3^+ \rightarrow (CF_3COCl)_2{\cdot}COCl^+ + CF_3$	0.38
$(CF_3COCl)_2^+ \rightarrow CF_3COCl{\cdot}CF_3CO^+ + Cl$	−0.05 (0.09)
$(CF_3COCl)_3^+ \rightarrow (CF_3COCl)_2{\cdot}CF_3CO^+ + Cl$	−0.09
$(CF_3COCl)_2^+ \rightarrow CF_3COCl{\cdot}CF_3^+ + COCl$	0.12 (0.24)
$(CF_3COCl)_3^+ \rightarrow (CF_3COCl)_2{\cdot}CF_3^+ + COCl$	0.04
$(CF_3COCl)_2^+ \rightarrow CF_3COCl{\cdot}CF_2COCl^+ + F$	1.20 (1.36)
$(CF_3COCl)_3^+ \rightarrow (CF_3COCl)_2{\cdot}CF_2COCl^+ + F$	1.42
$(CF_3COCl)_3^+ \rightarrow CF_3COCl{\cdot}CFCCl_2^+ + CF_4 + CO_2 + F$	1.82
$CF_3COCl + e^- \rightarrow Cl^- + CF_3CO$	−0.23 (−0.15)
$CF_3COCl + e^- \rightarrow CF_3^- + CO + Cl$	1.53 (1.62)
$CF_3COCl + e^- \rightarrow CF_3Cl^- + CO$	−0.55 (−0.47)
$CF_3COCl + e^- \rightarrow COCl^- + CF_3$	−0.20 (−0.08)
$CF_3COCl + e^- \rightarrow F^- + CF_2COCl$	1.60 (1.61)
$(CF_3COCl)_2 + e^- \rightarrow CF_3COCl_2^- + CF_3CO$	−0.79 (−0.85)
$(CF_3COCl)_3 + e^- \rightarrow (CF_3COCl)_2{\cdot}Cl^- + CF_3CO$	−0.78
$(CF_3COCl)_2 + e^- \rightarrow CF_3COCl{\cdot}CF_3^- + COCl$	0.27 (0.31)
$(CF_3COCl)_3 + e^- \rightarrow (CF_3COCl)_2{\cdot}CF_3^- + COCl$	0.22
$(CF_3COCl)_3 + e^- \rightarrow CF_3COCl{\cdot}Cl_2^- + 2CF_3CO$	2.27

the bond weakens considerably, prolonging from 1.56 Å to 2.09 Å (in agreement with the high experimental yield of CF_3^+ and $COCl^+$ ions). In the optimized ion, the charge is distributed almost equally, with 0.47*e* and 0.53*e* predicted for CF_3 and for COCl moieties, respectively. The energies of the most important dissociation channels are collected in Table 1, the low dissociation energies match nicely the experimental observations. The appearance of CF_3CO^+, CF_3^+ and $COCl^+$ can be explained by direct dissociation of a covalent bond, CF_2Cl^+ and CF_2^+ require a transfer of a chlorine or fluorine atom prior to the dissociation.

The electron-impact ionization can be described by the Binary–Encounter–Bethe (BEB) model in the formalism developed by Kim and co-workers.[35] In this model, the total ionization cross section is given as the sum of cross sections for ionization from occupied molecular orbitals, $\sigma_{tot} = \sum_i^{MOs} \sigma_i$. The individual σ_i's can be evaluated from orbital energies and kinetic energies by a semi-empirical formula.[35,36] These orbital σ_i's contributions, evaluated at 70 eV electron energy, are shown as Fig. S10 in the ESI.† A similar effect as was observed for a different fluorinated molecule in ref. 36 can be seen: the ionization from HOMO does not dominate the cross section, rather, the ionization from many molecular orbitals contributes significantly. This means that the cation is produced in many electronically excited states. Most probably, these undergo an

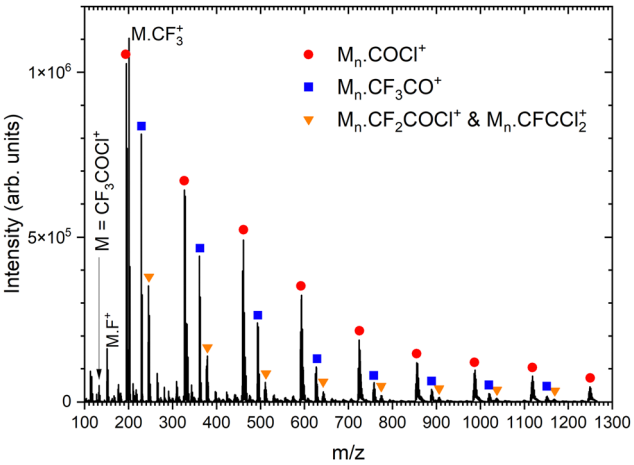

Fig. 3 The mass spectrum of $(CF_3COCl)_N$ clusters ionized at 70 eV electron energy. The clusters are produced in co-expansion of CF_3COCl molecules with Ar buffer gas at the expansion pressure of 3.8 bar.

ultrafast internal conversion into the ground cation state which is left vibrationally hot and fragments statistically.[36] Together with the low reaction energy for Cl evaporation (0.2 eV), this explains the low yield of the parent ion in the experimental spectrum.

Next, we generate $(CF_3COCl)_N$ clusters by co-expanding the CF_3COCl molecules with Ar buffer gas. Several expansion pressures were exploited and the spectra were qualitatively the same (see Fig. S1 in ESI†), therefore we show only the spectrum recorded at the highest used stagnation pressure of 3.8 bar corresponding to the largest produced clusters, see Fig. 3. In the mass range up to the monomer mass m/z = 132, the cluster spectra are very similar to the spectrum of the molecule (see Fig. S2 in ESI†). Three significant cluster ion series are labeled in Fig. 3: red circles denote the $M_n{\cdot}COCl^+$ series (M = CF_3COCl), blue squares label $M_n{\cdot}CF_3CO^+$, and orange triangles can correspond to $M_n{\cdot}CF_2COCl^+$ and/or $M_n{\cdot}CFCCl_2^+$. The ambiguity in the assignment of the last series arises from the mass coincidence (^{19}F plus ^{16}O coincides with ^{35}Cl). This could, in principle, be resolved by isotope contributions, namely ^{35}Cl and ^{37}Cl.

The cluster ions contain the ^{35}Cl and ^{37}Cl isotopes in a ratio corresponding to their natural abundances, which is $^{35}Cl : {}^{37}Cl$ = 0.76 : 0.24. Depending on the number of Cl atoms in the cluster, we can calculate the relative intensities of the isotope peaks that follow the binomial distribution (see ESI,† for details). In Fig. 4, we show the details of the ambiguous series $M_n{\cdot}R^+$, R = CF_2COCl or $CFCCl_2$ for n = 1–3, and we compare the peak intensities to the calculated abundances of the isotopes (symbols) assuming both assignments. The calculated isotope abundances are normalized to the maximum peak intensity in the corresponding group. The first mass peak group for n = 1 agrees better with the R = CF_2COCl assignment, while for n = 2 and 3, the isotope abundances for $M_n{\cdot}R^+$ with R = $CFCCl_2$ fit the spectrum better. In Fig. S3 and S4 in the ESI,† we demonstrate that the assignment using isotope ratios works well for the unambiguously assigned series $M_n{\cdot}COCl^+$ and $M_n{\cdot}CF_3CO^+$.

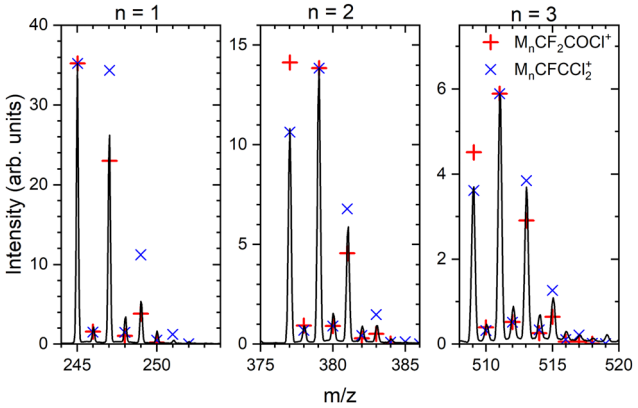

Fig. 4 Details of the mass spectrum of $(CF_3COCl)_N$ clusters for the ambiguous series $M_n{\cdot}R^+$ where R = CF_2COCl or $CFCCl_2$ (orange triangles in Fig. 3). Symbols indicate the calculated abundances of the isotopes normalized to the maximum peak within each group.

Therefore, we assume that the first group of mass peaks labeled by orange triangles in Fig. 3 corresponds mainly to $M{\cdot}CF_2COCl^+$ and the other mass peaks can be assigned to $M_n{\cdot}CFCCl_2^+$, $n \geq 2$, series, although a contribution of both series in all mass peaks cannot be excluded.

There is also a series corresponding to $M_n{\cdot}CF_3^+$. The first member of the series, $M{\cdot}CF_3^+$ at m/z = 201, is the labeled maximum peak in Fig. 3. The following $M_n{\cdot}CF_3^+$, $n > 1$, ion peaks have intensities comparable with the $M_n{\cdot}CFCCl_2^+$ series (orange triangles). The analysis is complicated by the isotopologue contribution of the major $M_n{\cdot}COCl^+$ ions as shown in ESI† (Fig. S5), but the contribution of the $M_n{\cdot}CF_3^+$ series is relatively small with the major contribution originating just from the first $M{\cdot}CF_3^+$ peak. The relative intensities of the cluster ion series $M_n{\cdot}COCl^+$, $M_n{\cdot}CF_3CO^+$, $M_n{\cdot}CF_3^+$, and $M_n{\cdot}CFCCl_2^+$ ($M_n{\cdot}CF_2COCl^+$) could be estimated to 46%, 25%, 20%, and 9%, respectively. These estimates should be considered with caution in view of relatively high spectra congestion, mass coincidences and ambiguities in the peak assignments. Nevertheless, the three major molecular fragments CF_3CO^+, CF_3^+, and $COCl^+$ are reflected in the cluster ion series, though in different ratios.

There are other minor series in the spectra, which could not be assigned, however, their contribution is small (see Fig. S6 in ESI,† for the fully resolved spectrum). Worth noting is the absence of non-fragmented cluster ions M_n^+, *i.e.*, $(CF_3COCl)_n^+$, in the spectrum, which points to the fact that the molecule is prone to a strong fragmentation after the electron ionization apparent from the mass spectrum of the isolated molecule, and even the cluster environment does not hinder this fragmentation.

Quantum chemical calculations show that the most stable structures of positively charged oligomers are often considerably reconstructed, see Fig. 1. Apart from simple dissociation of a CF_3COCl unit into CF_3 and COCl that are then stabilized in the cluster, we see also more fundamental reconstruction, *e.g.*, formation of FClC–CFCl or formation of a CO molecule. Still, we consider intact CF_3COCl oligomers to be the most probable moieties present in the experiment due to kinetic reasons. The adiabatic ionization energy of the neutral dimer and trimer is predicted to be 11.3 eV and 11.1 eV, respectively (CCSD//B3LYP-D3 level), Table 1.

With respect to the observed fragments, the presence of two main fragments, namely $M_n{\cdot}COCl^+$ and $M_n{\cdot}CF_3CO^+$, can be explained by direct dissociation of CF_3 and Cl, respectively, with reaction energies close to 0 eV. The electronic structure of the products can be described as $COCl^+$ and CF_3CO^+ stabilized by the cluster environment; the fact that no cluster reconstruction is required can contribute to the high experimental yield of these ions. As to $M_n{\cdot}CF_2COCl^+$, formation of a five-membered ring is predicted upon F atom dissociation as shown in (Fig. 1b); the respective formation energies lie below 2 eV (Table 1) for both dimers and trimers. Our calculations show that $M_n{\cdot}CF_2COCl^+$ and $M_n{\cdot}CFCCl_2^+$ fragments could be connected as they share the dissociation of F in the first place. For the second ion fragment, CF_4 and CO_2 molecules have to leave the cluster in the subsequent reaction.

The formation of the $M_n{\cdot}CF_3^+$ ions is predicted to proceed through a direct dissociation process and reconstruction into the $CF_3CClOCF_3^+$ ion as shown in (Fig. 1b), possibly leading to the lower $M_n{\cdot}CF_3^+$ abundance despite its low reaction energy and the fact that the CF_3^+ ion is the most abundant fragment in the monomer ionization. Finally, the very low reaction energies that even reach negative values for Cl dissociation explain the absence of M_n^+ clusters in the experimental mass spectra.

3.3 Negative ions

3.3.1 DEA of the CF_3COCl molecule. We start again with the results obtained for the beam of isolated molecules produced in co-expansion with helium. Since the electron attachment is very sensitive to the electron energy, the energy was scanned as the mass spectra were measured, as outlined in the Experimental section. Therefore, the results are presented in the form of a 2D intensity map shown in Fig. 5a. Some of the vertical traces corresponding to particular m/z are labeled by the corresponding negative fragment ion assignments. Although the 2D maps provide a convenient overview of the mass spectra energy dependence, a better quantitative analysis is obvious from the mass spectra shown in (Fig. 5b and c) where the long acquisitions at particular electron energies of 1.8 eV and 5.6 eV are shown.

There are two pronounced fragments produced in the DEA to the CF_3COCl molecule; namely Cl^- generated preferentially at low electron energies below 3 eV and CF_3^- that appear above 3 eV with a maximum between 5 and 6 eV, Fig. 6. Some much weaker fragments appear in the spectra shown in Fig. 5 upon closer inspection, especially at low electron energy, *e.g.*, CF_3Cl^-, $COCl^-$ and F^- with their energy dependence given also in Fig. 6. Further ions labeled in Fig. 5b are either negligible ($CFCOCl^-$, $C_2F_3^-$) or are obviously generated from dimers present in the molecular beam since they contain two oxygen atoms (grey labels in Fig. 5b). The energy-dependent ion yields in Fig. 6 show that dominant Cl^- (black) are produced at very low energies possibly with maximum at zero. There is a second much lower maximum at around 5.4 eV and possibly a weak

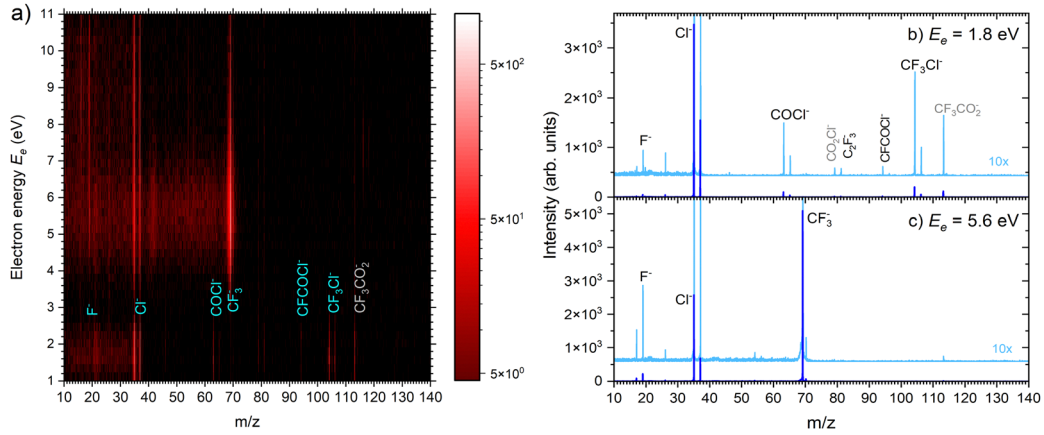

Fig. 5 (a) 2D mass spectra of negative ions produced by electron attachment to CF_3COCl molecules at different electron energies. (b) and (c) Mass spectra at two different electron energies.

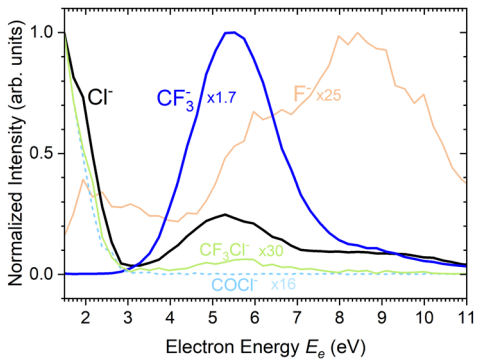

Fig. 6 Electron energy dependence of the negative ion yield in the DEA to CF_3COCl molecules.

shoulder at around 9–10 eV. CF_3^- ions (blue) are produced only at the higher energies of around 5.4 eV with a tail towards 9 eV suggesting a similar process to the Cl^- second peak. The other fragments are much less populated. Note that the energy-dependent ion yields shown in Fig. 6 have been normalized to the maximum (the multiplication factors are outlined by the corresponding lines). The CF_3Cl^- (light green) and $COCl^-$ (dashed light blue) ions also exhibit the maximum at low energies, and the former ion is also observed around 5.4 eV. The F^- ion (light orange) seems to have a different dependence with a wide maximum at around 8–9 eV and a shoulder at 6 eV (a low-energy peak at around 2 eV is uncertain due to low intensity).

The calculated adiabatic electron affinity of CF_3COCl is 1.04 eV. Upon electron attachment, an electron is added into the π* orbital of the C═O bond. The additional charge leads to the C–Cl bond prolongation to 2.18 Å. In the resulting moiety, $[CF_3CO\cdots Cl]^-$, the charge is almost equally distributed on CF_3CO (–0.45*e*) and Cl (–0.55*e*). Such a molecular anion is not experimentally observed in the binary electron collisions with isolated CF_3COCl since excess energy leads either to electron detachment or to the fragmentation of the complex (dissociative electron attachment, DEA).

According to the calculated reaction energies (Table 1), there are three exothermic DEA channels. Interestingly, the most energetically favorable one, formation of CF_3Cl^-, is experimentally observed to be rather weak. We ascribe its low cross section to the necessity for a complex atomic rearrangement on the resonant potential energy surface. On the other hand, Cl^- and $COCl^-$ can be formed by breaking a single bond and have similar calculated exothermicities (0.15 eV *vs.* 0.08 eV). Also, CF_3Cl^- can dissociate into $CF_3 + Cl^-$, requiring only 0.53 eV.

A combination of effects can contribute to the fact that the Cl^- yield is much higher (approximately by a factor of 16). The first one is the involved resonant state, especially its dissociative direction. We can roughly estimate the energy of the π* (C═O) resonance (*i.e.*, the vertical attachment energy at the geometry of the neutral) using the empirical relation between the energy of the unoccupied molecular orbital and the energy of the corresponding resonance. The empirical relation of Chen and Gallup[37] [$E_{res} = (E_{MO} - 2.33\ eV)/1.31$] predicts that adding an electron to the LUMO (E_{MO} = 2.31 eV) yields an E_{res} value very close to zero. It thus corresponds to a state which is very weakly bound or to a resonance with energy close to 0 eV. This is clearly the state involved in the low-energy Cl^- and $COCl^-$ production. Upon visual inspection of the LUMO (Fig. S11 in ESI†), it is clear that the antibonding plane crosses the C–Cl bond, while the C–C bond is in a bonding plane. This hints that upon the formation of the π* (C═O) resonance, the C–Cl bond will be promptly cleaved. The cross section for the cleavage of this bond can be further enhanced by the bending motion of the Cl atom from the plane defined by the CCO atoms. Such bending will mix the π* (C═O) resonance with a higher-lying σ* (C═O) state, such mixing strongly increases the DEA cross section.[38–40] Also, the reduced mass of the $CF_3CO\cdots Cl^-$ system is 25.7 amu, while that of the $CF_3\cdots COCl^-$ system is 32.9 amu (for the ^{35}Cl isotope). The dissociation in the latter case will be thus slower, providing more time for the electrons to autodetach.[41] This leads to lowering of the DEA cross section in the $COCl^-$ channel. Finally, the $COCl^-$ ion is a weakly bound complex, $CO\cdots Cl^-$, and might easily dissociate to $CO + Cl^-$ with a calculated reaction energy of 0.14 eV.

Formation of CF_3^- has a calculated threshold of 1.62 eV. The experimental signal peaks appear at around 5.4 eV. The UV-VIS spectrum[5] supported by theoretical calculations[10] exhibits a maximum at around 4.9 eV. Thus, the incoming electron can excite the molecule and the observed peak can correspond to a core-excited shape resonance (their formation can be possibly enhanced by a dipole moment of the excited states[42,43]). The DEA peaks visible at about 8–10 eV could correspond to the core-excited resonances that have higher excited states[10] as the parent states.

3.3.2 Electron attachment to clusters. Fig. 7 shows the 2D mass spectrum and electron energy dependence after electron attachment to the $(CF_3COCl)_N$ clusters generated under the same expansion conditions as the positive ion spectrum in Fig. 3. The molecular part of the spectrum is essentially the same as that for the DEA of the isolated molecule shown in Fig. 5. The major cluster fragments, labeled in Fig. 7, are $M_n{\cdot}Cl^-$ that prevail at higher electron energies but one can see in Fig. 8 that the spectrum is dominated by the cluster ions M_n^- (*i.e.*, $(CF_3COCl)_n^-$) at lower energies below 3 eV.

Fig. 8 shows the mass spectra at specific electron energies of (a) 1.7 eV, (b) 5.0 eV and (c) 8.0 eV. The major cluster ion fragment series are $M_n{\cdot}Cl^-$ and M_n^- mentioned above. Also an interesting series with molecular chlorine $M_n{\cdot}Cl_2^-$ exhibits appreciable abundances at higher energies. However, $M_n{\cdot}Cl_2^-$ overlaps with $M_n{\cdot}CF_3^-$ due to isotope contributions (Cl_2^- corresponds to m/z = 70 for the ^{35}Cl isotope, and CF_3^- to m/z = 69). The two series differ by the number of Cl atoms, therefore a detailed analysis is possible using the natural isotope abundances as outlined for the positive ions. It shows that both $M_n{\cdot}Cl_2^-$ and $M_n{\cdot}CF_3^-$ series are present in the spectra (see Fig. S7 and S8 in the ESI†).

We identify further less abundant ion series in the spectra upon close analysis as well. For example, a group of mass peaks corresponding to $M_n{\cdot}CF_3CO^-$ at m/z = 229 is labelled in (Fig. 8b) at 5.0 eV. This peak and further smaller fragment series are shown in detailed spectra as shown in Fig. S9 in the ESI.† However, the abundance of these ions is relatively small.

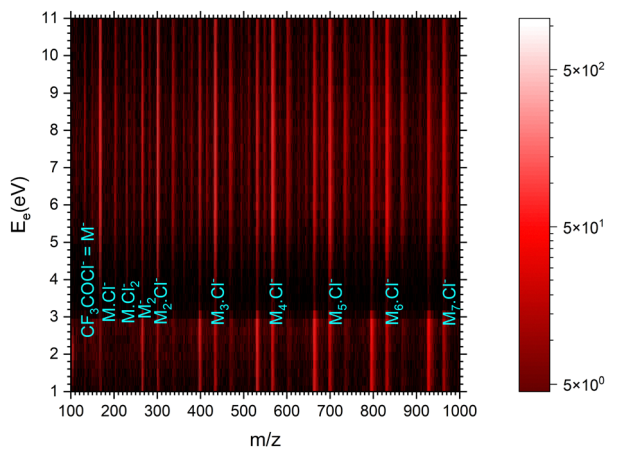

Fig. 7 The 2D mass spectrum and electron energy dependence after the electron attachment to the $(CF_3COCl)_N$ clusters.

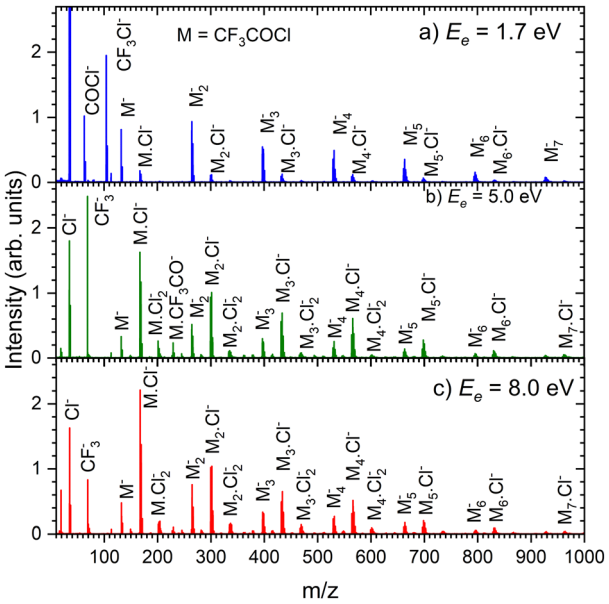

Fig. 8 The mass spectra at specific electron energies of (a) 1.7 eV, (b) 5.0 eV and (c) 8.0 eV.

Finally, we discuss the electron energy dependent ion yield for several cluster ion fragments shown in Fig. 9. The top panels show the negative ion yield of (a) Cl^- and (b) CF_3^- fragments (orange lines) in comparison with the yields of the same ions from the DEA of isolated molecules (black). The high-energy tails of the cluster spectra suggest that in clusters, processes at somewhat higher energies can also contribute to the generation of these ions. Panels (c) and (d) below show the spectra for the $M_n{\cdot}Cl^-$ and $M_n{\cdot}CF_3^-$ ions respectively. The shape of the spectra is independent of the cluster ion size n. A comparison of Fig. 9c and d with Fig. 9a and b, respectively, suggests that the main maxima in the top spectra are due to the isolated molecules in the beam and the Cl^- and CF_3^- fragments from the clusters are produced at higher energies. The low-energy maximum for Cl^- seems to be strongly suppressed in the clusters. Finally, the bottom row in Fig. 9e and f shows the spectra for M_n^- and $M_n{\cdot}Cl_2^-$ fragments. The M_n^- ions are produced at low energies. The broad peak at higher energies might be due to the self-scavenging processes in clusters,[29] where the incoming electron excites a CF_3COCl molecule, loses its kinetic energy and attaches as the slow electron. The $M_n{\cdot}Cl_2^-$ ions are formed at higher electron energies due to the extra energy required to rearrange the molecules (see below).

The calculated adiabatic electron affinity of the CF_3COCl dimer and trimer is 1.32 eV and 1.58 eV, respectively (CCSD//B3LYP-D3). As already hinted through the experiments, the cluster environment might prevent the Cl^- pre-dissociation. Although Cl^- could be formed in the cluster, a cluster conformation with intact CF_3COCl units is slightly more stable (Fig. 1).

In the case of $CF_3COCl_2^-$, our calculations suggest that a C–Cl bond is formed, see Fig. 1, the formation of the ion upon electron attachment is exothermic in both dimer and trimer

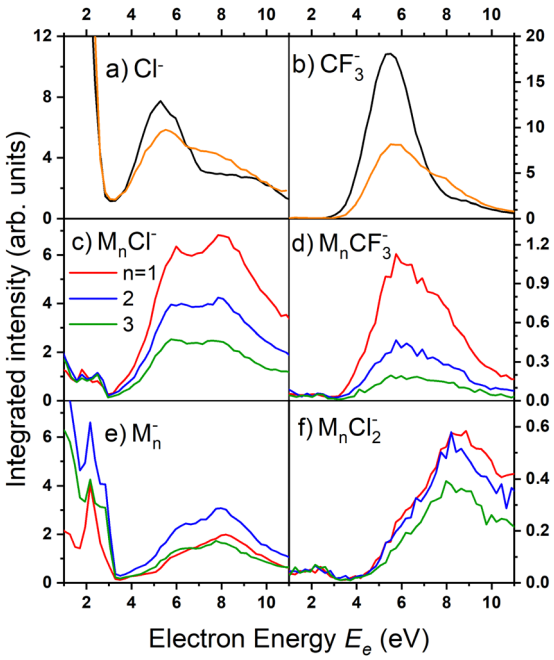

Fig. 9 The electron energy dependence of the negative ion yield for several fragments of the electron attachment to the $(CF_3COCl)_N$ clusters. The black lines in the top panels correspond to the spectra of isolated molecules for comparison.

(Table 1). For the $M_2{\cdot}Cl^-$ ion, a Cl^- anion is predicted to lie next to the CF_3COCl molecules. The formation of $M_n{\cdot}CF_3^-$ is again predicted to be connected to cluster reconstruction, forming a $CF_3C(Cl)OCF_3^-$ unit. The $M_n{\cdot}Cl_2^-$ anion can be produced by the dissociation of two CF_3CO units, forming a $CF_3COCl_2\cdots Cl^-$ cluster at an energy of about 2.3 eV.

4 Conclusions

We performed a molecular beams study of trifluoroacetyl chloride and its clusters, analyzing their behavior by interaction with electrons.

For an isolated molecule, ionization leads to the weakening the C–C bond, yielding CF_3^+ or $COCl^+$ fragment ions. Breaking of the C–Cl bond leads to the major fragment ion CF_3CO^+, however, the sum of CF_3^+ and $COCl^+$ ion yields exceeds the CF_3CO^+ yield significantly, suggesting that the C–C bond dissociation is the primary channel. On the other hand, the electron attachment primarily breaks the C–Cl bond leading to Cl^- dominating at low electron energies below 3 eV, and CF_3^-, which is the major channel at higher energies above 4 eV.

For clusters, a typical feature is their thermodynamic instability, with cluster reconstruction often predicted to be favorable by our genetic algorithm search. In cationic clusters, two main series are observed upon ionization, $M_n{\cdot}COCl^+$ and $M_n{\cdot}CF_3CO^+$, both formed through direct dissociation. In the case of minor fragments, considerable cluster reconstruction is predicted, most probably contributing to their low experimental yield.

For anions, stabilized molecular M_n^- clusters dominate the mass spectra at low energies below 3 eV. Also dissociation of the C–Cl bond plays a role at low energies forming $M_n{\cdot}Cl^-$ fragment ions, which become the dominant species at higher electron energies above 4 eV. The dissociation of the C–C bond can occur as well at these higher energies, forming $M_n{\cdot}CF_3^-$. At higher energies, $M_n{\cdot}Cl_2^-$ cluster ions also occur.

In terms of atmospheric relevance we stress two findings: (i) the gas-phase molecule is very fragile with respect to the electron impact, both the positive ionization and electron attachment mass spectra are fragmentative, and (ii) the major cationic fragment in the gas phase is CF_3CO^+, with its necessary neutral counterpart being the Cl radical. Upon aggregation, the anion dissociation pathways are considerably suppressed and the intact molecular cluster anions are dominant. The cationic pathways are not influenced by clustering as strongly as the anionic ones, even though the chlorine-producing channel ($M_n{\cdot}CF_3CO^+$) is not the most dominant fragment progression in clusters.

Author contributions

B. Kocábková: data curation, investigation, formal analysis, and visualization; J. Ďurana: investigation, formal analysis, and visualization; J. Rakovský: investigation; A. Pysanenko: investigation; V. Poterya: investigation; J. Fedor: writing – review and editing, and validation; M. Ončák: conceptualization, writing original draft, formal analysis, visualization, validation; and M. Fárník: conceptualization, writing original draft, formal analysis, visualization, validation, and funding acquisition.

Conflicts of interest

There are no conflicts to declare.

Acknowledgements

This work has been supported by the Czech Science Foundation project Nr. 21-07062S, MEYS CZ project Nr. LTC20067. The collaboration has been supported by COST Action CA18212 MD-GAS, supported by COST (European Cooperation in Science and Technology). The computational results presented have been achieved using the HPC Infrastructure LEO of the University of Innsbruck.

Notes and references

1 A. Ravishankara, A. Turnipseed, N. Jensen, S. Barone, M. Mills, C. Howard and S. Solomon, *Science*, 1994, **263**, 71–75.
2 O. Wild, O. Rattigan, R. Jones, J. Pyle and R. Cox, *J. Atmos. Chem.*, 1996, **25**, 167–199.
3 J. Francisco, *Chem. Phys.*, 1992, **163**, 27–36.
4 J. B. Burkholder, R. Cox and A. Ravishankara, *Chem. Rev.*, 2015, **115**, 3704–3759.

5 O. Rattigan, O. Wild, R. Jones and R. Cox, *J. Photochem. Photobiol., A*, 1993, **73**, 1–9.
6 M. M. Maricq and J. J. Szente, *J. Phys. Chem.*, 1995, **99**, 4554–4557.
7 M. R. McGillen and J. B. Burkholder, *Chem. Phys. Lett.*, 2015, **639**, 189–194.
8 R. Meller and G. K. Moortgat, *J. Photochem. Photobiol., A*, 1997, **108**, 105–116.
9 Y. Hao, L. Liu and W.-H. Fang, *J. Chem. Phys.*, 2021, **154**, 244303.
10 J. Janoš, I. S. Vinklárek, J. Rakovský, D. P. Mukhopadhyay, B. F. E. Curchod, M. Fárník and P. Slavíček, *ACS Earth Space Chem.*, 2023, **7**, 2275–2286.
11 F. E. Malanca, G. A. Argüello, E. H. Staricco and R. P. Wayne, *J. Photochem. Photobiol., A*, 1998, **117**, 163–169.
12 C. Berney, *Spectrochem. Acta*, 1964, **20**, 1437–1449.
13 J. Durig, A. Fanning, T. Sheehan and G. Guirgis, *Spectrochim. Acta, Part A*, 1991, **47**, 279–289.
14 K. I. Gobbato, C. Leibold, S. Centeno, C. O. Della Védova, H.-G. Mack and H. Oberhammer, *J. Mol. Struct.*, 1996, **380**, 55–61.
15 G. Bent, E. Zerrad, G. Trucks, K. Wiberg and L. Taing, *J. Phys. Chem. A*, 2000, **104**, 370–379.
16 I. A. Mironova, K. L. Aplin, F. Arnold, G. A. Bazilevskaya, R. G. Harrison, A. A. Krivolutsky, K. A. Nicoll, E. V. Rozanov, E. Turunen and I. G. Usoskin, *Space Sci. Rev.*, 2015, **194**, 1–96.
17 I. I. Fabrikant, S. Eden, N. J. Mason and J. Fedor, *Advances In Atomic, Molecular, and Optical Physics*, Elsevier Inc., Academic Press, 2017, vol. 66, pp. 545–657.
18 Q.-B. Lu and L. Sanche, *Phys. Rev. Lett.*, 2001, **87**, 078501.
19 Q.-B. Lu, *Proc. Natl. Acad. Sci. U. S. A.*, 2023, **120**, e2303048120.
20 Q.-B. Lu, *Phys. Rep.*, 2010, **487**, 141–167.
21 Q.-B. Lu, *Int. J. Modern Phys. B*, 2013, **28**, 1350073.
22 R. Müller and J. U. Grooss, *Int. J. Modern Phys. B*, 2014, **28**, 1482001.
23 D. Nuccitelli, K. Cowtan, P. Jacobs, M. Richardson, R. G. Way, A.-M. Blackburn, M. B. Stolpe and J. Cook, *Int. J. Modern Phys. B*, 2014, **28**, 1482003.
24 M. Fárník, *J. Phys. Chem. Lett.*, 2023, **14**, 287–294.
25 M. Fárník, J. Fedor, J. Kočišek, J. Lengyel, E. Pluharová, V. Poterya and A. Pysanenko, *Phys. Chem. Chem. Phys.*, 2021, **23**, 3195–3213.
26 M. Fárník and J. Lengyel, *Mass Spec Rev.*, 2018, **37**, 630–651.
27 J. Lengyel, A. Pysanenko, J. Kočišek, V. Poterya, C. Pradzynski, T. Zeuch, P. Slavíček and M. Fárník, *J. Phys. Chem. Lett.*, 2012, **3**, 3096–3109.
28 J. Kočišek, J. Lengyel and M. Fárník, *J. Chem. Phys.*, 2013, **138**, 124306.
29 J. Lengyel, J. Kočišek, M. Fárník and J. Fedor, *J. Phys. Chem. C*, 2016, **120**, 7397–7402.
30 J. Kočišek, A. Pysanenko, M. Fárník and J. Fedor, *J. Phys. Chem. Lett.*, 2016, **7**, 3401–3405.
31 S. Grimme, J. Antony, S. Ehrlich and H. Krieg, *J. Chem. Phys.*, 2010, **132**, 154104.
32 C. M. Breneman and K. B. Wiberg, *J. Comput. Chem.*, 1990, **11**, 361–373.
33 G. Schöpfer, M. Hütter, M. Gatt and M. Ončák, *Genetic Algorithms for Finding Molecules, (v1.0)*, **https://git.uibk.ac.at/c7441332/genetic-algorithms**.
34 M. J. Frisch, G. W. Trucks, H. B. Schlegel, G. E. Scuseria, M. A. Robb, J. R. Cheeseman, G. Scalmani, V. Barone, B. Mennucci, G. A. Petersson, H. Nakatsuji, M. Caricato, X. Li, H. P. Hratchian, A. F. Izmaylov, J. Bloino, G. Zheng, D. J. Sonnenberg, M. Hada, M. Ehara, K. Toyota, R. Fukuda, J. Hasegawa, M. Ishida, T. Nakajima, Y. Honda, O. Kitao, H. Nakai, T. Vreven, J. Montgomery, Jr., J. R. Peralta, F. Ogliaro, M. Bearpark, J. J. Heyd, E. Brothers, K. N. Kudin, V. N. Staroverov, R. Kobayashi, J. Normand, K. Raghavachari, A. Rendell, J. C. Burant, S. S. Iyengar, J. Tomasi, M. Cossi, N. Rega, J. M. Millam, M. Klene, J. E. Knox, J. B. Cross, V. Bakken, C. Adamo, J. Jaramillo, R. Gomperts, R. E. Stratmann, O. Yazyev, A. J. Austin, R. Cammi, C. Pomelli, J. W. Ochterski, R. L. Martin, K. Morokuma, V. G. Zakrzewski, G. A. Voth, P. Salvador, J. J. Dannenberg, S. Dapprich, A. D. Daniels, O. Farkas, J. B. Foresman, J. V. Ortiz, J. Cioslowski and D. J. Fox, *Gaussian 16 Revision A.03*, Gaussian Inc., Wallingford CT, 2016.
35 W. Hwang, Y.-K. Kim and M. E. Rudd, *J. Chem. Phys.*, 1996, **104**, 2956.
36 M. Rankovič, J. Chalabala, M. Zawadzki, J. Kočišek, P. Slavíček and J. Fedor, *Phys. Chem. Chem. Phys.*, 2019, **21**, 16451.
37 D. Chen and G. A. Gallup, *J. Chem. Phys.*, 1990, **93**, 8893–8901.
38 P. Nag, M. Tarana and J. Fedor, *Phys. Rev. A*, 2021, **103**, 032830.
39 M. Zawadzki, M. Čížek, K. Houfek, R. Čurík, M. Ferus, S. Civiš, J. Kočišek and J. Fedor, *Phys. Rev. Lett.*, 2018, **121**, 143402.
40 T. P. R. Kumar, P. Nag, M. Rankovič, J. Kočišek, Z. Mašín and J. Fedor, *J. Phys. Chem. Lett.*, 2022, **13**, 11136–11142.
41 R. Janečková, D. Kubala, O. May, J. Fedor and M. Allan, *Phys. Rev. Lett.*, 2013, **111**, 203201.
42 Z. Li, M. Ryszka, M. M. Dawley, I. Carmichael, K. B. Bravaya and S. Ptasińska, *Phys. Rev. Lett.*, 2019, **122**, 073002.
43 J. Fedor, *Phys. Rev. Lett.*, 2020, **124**, 199301.

